

# International Conference on Space Optics—ICSO 2022

Dubrovnik, Croatia

3–7 October 2022

*Edited by Kyriaki Minoglou, Nikos Karafolas, and Bruno Cugny,*



## *Impact of atmospheric refraction on free-space optical communications pointing*



# Impact of atmospheric refraction on free-space optical communications pointing

B. Benammar, G. Artaud  
CNES, Centre National d'Etudes Spatiales (French Space Agency)  
18 avenue Edouard Belin, 31400 Toulouse, France

## ABSTRACT

This paper presents an analysis of the angular offsets due to atmospheric refraction for ground-space Free Space Optical (FSO) communications. The paper presents a theoretical framework for modelling the optical atmospheric refraction index as well as a set of reference atmospheres refraction indexes representative of different climates. The developed framework is then applied to the estimation of both elevation and nadir angles at different wavelengths. Results show that the offsets of apparent elevation and nadir angles for systems using pointing wavelengths outside communication bands (typically vis. 500nm or IR 808nm pointing wavelengths for 1550nm communication wavelength) can be significant. For example, offsets of 60 $\mu$ rad of apparent elevation angle (at 5° geometric link elevation) can be experienced when the pointing wavelength is at 500nm and the communication wavelength is at 1550nm.

**Keywords:** Atmospheric refraction, pointing, propagation, free space optical communications

## 1. INTRODUCTION

Free Space Optical (FSO) communications have been increasingly investigated as alternative or complementary technologies to existing radiofrequency satellite communications systems. Indeed, optical transmissions offer interesting data rates with regard to the actual and foreseen radiofrequency bands for both telecommunications and data telemetry. However, optical links are subject to stronger atmospheric impairments. In the C and L band (around 1.55 $\mu$ m), optical signals are affected by molecular absorption, clouds and aerosols scattering as well as refractivity. Refractivity includes slow variations of refractive index, which induces path bending, as well as fast variations of the index of refraction resulting in the well-known phenomenon of optical turbulence.

In this paper, we are interested in the impact of the slow varying atmospheric refractivity on the propagation of optical signals and its implications on pointing strategies for the case of LEO Direct To Earth (DTE) communications. Earth's atmosphere refractivity originates from the spatial variation of the refractive index along the optical path. Atmospheric refractivity induces ray bending which increases the path length usually and thus affecting delay-sensitive systems such as radio-navigation services as well as Satellite Laser Ranging (SLR) and FSO frequency and time transfer techniques. Atmospheric refractivity can also have implications on pointing considerations for FSO communications. Indeed, the optical refractive index being wavelength dependent, signals with different wavelengths follow different optical paths and thus have different angles of arrival. It is thus important to quantify the difference between angles of arrival especially when the satellite pointing uses a different wavelength with regard to communications wavelengths.

To do so, multiple approaches can be used to compute the refracted angles in the atmosphere. The first one is a simplistic version where Earth's atmosphere is modelled as a single layer of refractive index as in recommendation ITU-R P.1621-2 [1]. This method gives a rough estimate of the apparent elevation angle only. A more refined estimation of slant path refracted angles models Earth's atmosphere as multiple concentric layers of decreasing refractive indexes. A similar approach is used in recommendation ITU-R P.676-12 [2] for the computation of gaseous specific attenuation for radiofrequency links. However, the presented formulas are more oriented towards the excess path length computation and rely on the step-by-step computation of refracted angles for a given numerical values of refractive index. Moreover, this recommendation is more oriented towards the computation of excess path length for attenuation considerations. Thus, although presenting some useful formulas to compute the elevation angle, the apparent angle is not a direct result. Authors in [4] have also investigated the impact of refraction on multiple wavelength systems but the analysis was carried out for horizontal optical link.

In this paper, we present a different computation method which allows the estimated of refracted angles for both numerical values of refractive index as well as theoretical vertical distribution of the refractive index when available. This approach has been presented in [3], but applied to radiofrequency systems using theoretical formulas of radiofrequency refractive index to compute the refracted elevation angle. Thus, the results in [3] are not directly exploitable for optical links especially because radiofrequency and optical refractive indexes expressions are different. In this paper, we build on the formalism presented in [3] to generalize the computation of refracted angles to the computation of the nadir refracted angle which is a novel results to the authors' knowledge. We also exploit the results in different atmospheric conditions in order to analyse the sensitivity of refracted angles to climatic and seasonal variations.

The paper is organized as follows. Section 2 presents the system description as well as the theoretical framework for satellite refracted angles. In Section 3, we present the considered reference standard atmospheres and the corresponding refractive index profiles. Section 4 presents the analysis of elevation and nadir angles for different system wavelengths and Section 5 concludes with some remarks.

## 2. ATMOSPHERIC REFRACTION

### 2.1 System definition

The objective of this study is to evaluate the performance of pointing strategies for LEO satellite direct to earth communications using different wavelengths for the uplink pointing and the downlink communications. More specifically, we are interested in estimating the refracted angles of elevation -from Optical Ground Station (OGS)- and nadir -from satellite- in the presence of atmospheric refraction using realistic atmospheric refraction profiles for different wavelengths falling in the visible, infra-red, and L/C optical bands. To do so, we consider links between earth and a LEO platform as depicted in Figure 1.

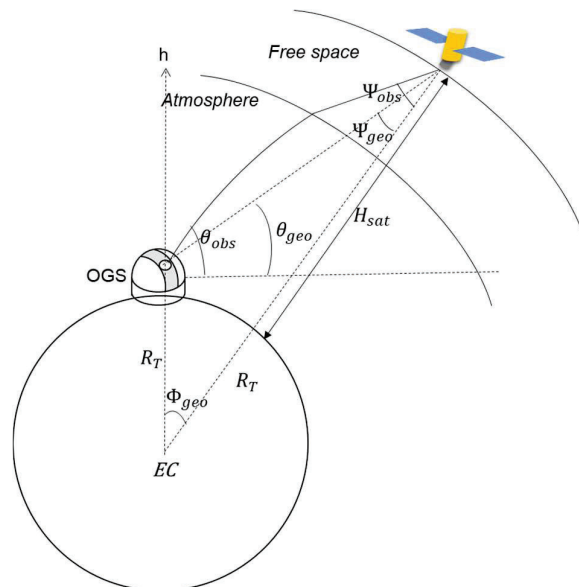


Figure 1: System configuration

The following assumptions and definitions are considered. Earth is assumed spherical with radius  $R_T$  and with center  $EC$  (Earth's Center).  $H_{sat}$  is the altitude of the satellite assumed having a circular orbit. All elevation and nadir angles are defined in a reference frame centered at the OGS.

In the sequel, geometric angles correspond to the angles in the absence of refraction, i.e. following geometrical considerations only. These angles are subscripted “geo”, and are defined as follows:

- Geometric elevation angle  $\theta_{geo}$  is the angle at which the OGS views the satellite with regard to OGS horizon
- Nadir angle  $\Psi_{geo}$  is the angle at which the satellite views the OGS with regard to its nadir and is defined as :

$$\Psi_{geo} = \sin^{-1} \left( \cos(\theta_{geo}) \frac{R_T}{R_T + H_{sat}} \right) \quad (1)$$

- Earth Centered (EC) angle  $\phi_{geo}$  is the angle between the zenith of OGS and the zenith of satellite viewed from Earth’s center and defined as :

$$\phi_{geo} = \sin^{-1}(\cos(\theta_{geo})) - \sin^{-1} \left( \cos(\theta_{geo}) \frac{R_T}{R_T + H_{sat}} \right) \quad (2)$$

In the presence of refractivity, optical rays bend along the propagation path until reaching the outer limit of the atmosphere and then propagate as direct rays towards and from the satellite. This results in apparent angles different from geometric angles. These apparent angles are referred to as “observed” angles and subscripted “obs” in the following. More specifically,  $\theta_{obs}$  refers to the observed elevation angle from OGS and  $\Psi_{obs}$  refers to the observed nadir angle from satellite.

### 2.2 Refraction laws

Optical refraction occurs for an incoming ray at the interface of two mediums with different refraction indexes. The simplest representation of optical refraction is the classical plane-parallel case as depicted in Figure 2.

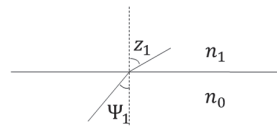


Figure 2: Plane parallel refraction

The incoming wave has an incidence angle  $\Psi_1$  in the  $n_0$  refractive index medium and an output angle  $z_1$  in the  $n_1$  refractive index medium. The relation between  $n_0, n_1, \psi_1$  and  $z_1$  by Snell-Descartes refraction law writes as follows:

$$n_0 \sin(\Psi_1) = n_1 \sin(z_1) \quad (3)$$

This implies that the ray bends towards the medium with the lower refraction index, as illustrated in the Figure 2 where we assume  $n_0 > n_1$ .

In a less simplistic case, assuming a ray propagating in a medium with radial symmetry such as the case of Earth’s atmosphere, refraction laws can also be developed building on the approximation of locally plane-parallel refraction between successive layers of atmosphere as represented in Figure 3.

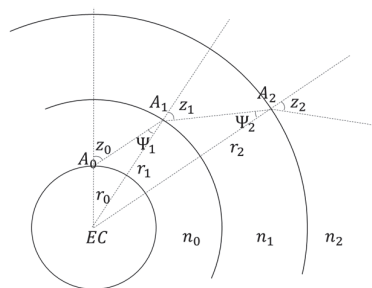


Figure 3 : Radial symmetry spherical refraction

In this case, Earth’s atmosphere is decomposed into successive layers with increasing radii  $r_0, r_1, r_2 \dots$  and decreasing refractive indexes  $n_0 > n_1 > n_2 > \dots$ .

At each interface "A<sub>i</sub>" ( $i \geq 1$ ) between layers with refraction indexes  $n_{i-1}$  and  $n_i$ , we use plane-parallel refraction as:

$$n_{i-1} \sin(\Psi_i) = n_i \sin(z_i) \tag{4}$$

Taking into account geometrical angles delimited by the triangle (EC, A<sub>i-1</sub>, A<sub>i</sub>), and using the sinus law of triangles, we can write:

$$\frac{r_i}{\sin(z_{i-1})} = \frac{r_{i-1}}{\sin(\psi_i)} \tag{5}$$

Using equations (4) and (5), the refraction at interface "A<sub>i</sub>" ( $i \geq 1$ ) writes as:

$$n_{i-1} r_{i-1} \sin(z_{i-1}) = n_i r_i \sin(z_i) \tag{6}$$

This formula leads to the well-established refraction law in polar coordinates as follows [3]:

$$\forall i \quad n_i r_i \sin(z_i) = \text{Constant} \triangleq A \tag{7}$$

In a continuous atmosphere defined by index of refraction  $n(r)$  at radius  $r$  from Earth’s center, this relation translates to the so-called “refraction constant”, noted A, described as follows :

$$A = r n(r) \sin(z) \quad \forall r > 0 \tag{8}$$

where  $z$  is the local zenith angle at the output of the layer at radius  $r$  from EC.

### 2.3 Observed elevation and nadir angles

Using the refraction theory presented above, we can derive the observed angles by integrating the differential refracted angles along the slant path. To do so, we consider the differentiation depicted in Figure 4.

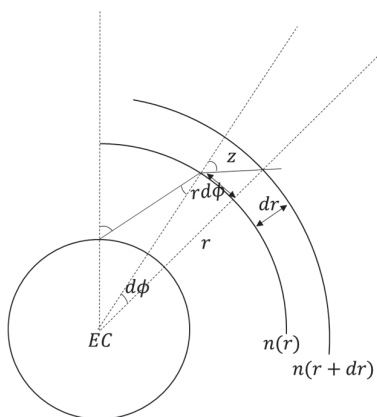


Figure 4 : Differential refraction

In this configuration, we assume that there is no variation of refractive index within the radial distance “dr”. Using the geometrical consideration between  $r d\phi$  and  $dr$ , it can be shown that the Earth-centered differential angle  $d\phi$  writes as:

$$d\phi = \frac{dr}{r} \tan(z) \tag{9}$$

Integrating over the slant path leads to:

$$\phi_{obs} = \int_{R_T}^{R_T+H_{sat}} \frac{1}{r} \tan(z) dr \quad (10)$$

where  $\phi_{obs}$  is the Earth center angle at which the ray intersects the satellite orbit after propagation between Earth's surface and satellite altitude. Using the expression of  $\tan(z)$  in equation (8) and the relation given in equation (10), it can be shown that the angle  $\phi_{obs}$  writes as:

$$\phi_{obs} = \int_{R_T}^{R_T+H_{sat}} \frac{A}{r\sqrt{n(r)^2r^2 - A^2}} dr \quad (11)$$

This formula relates the refraction vertical profile  $n(r)$  with the angle  $\phi_{obs}$  at which the transmitted ray intersects with the satellite orbit. In order for the optical ray to hit the satellite at its position on orbit, the observed EC angle needs to satisfy:  $\phi_{obs} = \phi_{geo}$  where  $\phi_{geo}$  is the Earth-centered geometrical angle defined in (2).

For a given link elevation  $\theta$ , we use the refraction constant defined in (8) to write:

$$A = R_T n(R_T) \cos(\theta) \quad (12)$$

In this case, the observed Earth-centered angle  $\phi_{obs}(\theta)$  writes as:

$$\phi_{obs}(\theta) = \int_{R_T}^{R_T+H_{sat}} \frac{R_T n(R_T) \cos(\theta)}{r\sqrt{n(r)^2r^2 - R_T^2 n(R_T)^2 \cos^2(\theta)}} dr \quad (13)$$

In this case, the elevation angle that allows the ray to reach the satellite  $\theta_{obs}$  should be solution to the equation:

$$\theta_{obs} \text{ satisfies } \phi_{obs}(\theta_{obs}) = \phi_{geo} \quad (14)$$

Similarly, expressing the refraction constant at the satellite level where the refractive index  $n(R_T + H_{sat}) = 1$  (since the satellite is in free space), one can write:

$$A = (R_T + H_{sat}) \sin(\Psi) \quad (15)$$

which allows to write the observed EC angle  $\phi_{obs}(\Psi)$  as follows :

$$\phi_{obs}(\Psi) = \int_{R_T}^{R_T+H_{sat}} \frac{(R_T + H_{sat}) \sin(\Psi_{obs})}{r\sqrt{n(r)^2r^2 - (R_T + H_{sat})^2 \sin^2(\Psi_{obs})}} dr \quad (16)$$

Then the nadir angle at which the satellite can view the OGS needs to be solution to:

$$\Psi_{obs} \text{ satisfies } \phi_{obs}(\Psi_{obs}) = \phi_{geo} \quad (17)$$

Equations in (13) and (16) could have a closed form if a theoretical expression of the index of refraction  $n(r)$  is available. If only numeric data are available, then numerical integration can be used to solve  $\theta_{obs}$  and  $\Psi_{obs}$ . This numerical integration consists of successive ray launching at different elevation and nadir angles and then testing the criteria given in (14) and (17).

An equivalent method to compute  $\Psi_{obs}$  is to compute the observed elevation angle  $\theta_{obs}$  and use formula of the constant of refraction defined in (8) to write:

$$A = R_T n(R_T) \cos(\theta_{obs}) = (R_T + H_{sat}) \sin(\Psi_{obs}) \quad (18)$$

It can be noted that in the absence of atmospheric refraction i.e.  $n(r) = 1 \forall r$ , this equation gives the relation between the geometrical elevation and nadir angle given in equation (1).

### 3. REFERENCE ATMOSPHERIC REFRACTION PROFILES

#### 3.1 Optical refractive index

The expression of the atmospheric refractive index depends on the electromagnetic region considered. For radiofrequency bands, the refractive index is assumed independent of the signal frequency but depends on atmospheric parameters such as pressure, temperature and humidity as described in recommendation ITU-R P.453-14 [6]. For optical bands, the refractive index depends on the signal wavelength as well as pressure and temperature.

Several models have been defined for the optical index of refraction. In this study, we consider the model defined in [5] where for « standard » conditions i.e. pressure  $P_s = 1013.25 \text{ hPa}$  and temperature  $T_s = 288.15 \text{ K}$ , the “standard” refractive index writes as:

$$n_s(\lambda) = 1 + 10^{-8} \left( 6432.8 + \frac{2949810}{146 - \lambda^{-2}} + \frac{25540}{41 - \lambda^{-2}} \right) \quad (19)$$

where  $\lambda$  is the wavelength expressed in  $\mu\text{m}$ . This expression can also be found in recommendation ITU-R P.1621-2 [1]. For other non-standard atmospheric conditions, i.e. for given pressure  $P$  and temperature  $T$ , the index of refraction writes as:

$$n(\lambda, P, T) = 1 + \frac{P}{P_s} \frac{T_s}{T} (n_s(\lambda) - 1) \quad (20)$$

where  $P$  is the pressure expressed in hPa and  $T$  the temperature expressed in K. It can be noted that this expression of refractive index is decreasing in terms of wavelength  $\lambda$ .

Recommendation ITU-R P.1621-2 preconizes a different scaling formula originating from fitting of data at the observatory of Mauna Kea, which is too specific for a general purpose model and is thus not considered in this paper.

#### 3.2 Reference standard atmospheres

Given the definition of the index of refraction in equation (19), one can derive vertical profiles of refractive index  $n(\lambda, h)$  if vertical profiles of pressure  $P(h)$  and temperature  $T(h)$  are available. These vertical atmospheric profiles can be derived analytically from the thermodynamics of the atmosphere or extracted from numerical models and/or radio sounded databases. In this study, we considered using numerical vertical profiles available in the literature. Numerous databases provide reference atmospheres for radiative transfer needs such as Thermodynamic Initial Guess Retrieval (TIGR) database but also for radiofrequency satellite systems such as ITU-R P.835-6 [7], which is the reference database considered for this study.

These standard atmospheres are vertical atmospheric profiles representative of different climate and seasons types on the globe and are summarized in the following:

- Profile « Global Mean Annual » (GMA): a mean profile over the globe having standard pressure and temperature at the surface corresponding to the standard values previously defined in Section 3.1 i.e.  $P_s = 1013.25 \text{ hPa}$  et  $T_s = 288.15 \text{ K}$ .
- Profile « Low Latitudes » (LL): a mean profile characterizing latitudes lower than  $22^\circ$ . The seasonal variability of such climatic regions is insignificant and thus only an annual mean profile is defined for these low latitudes.
- Profile « Mid Latitude Summer » (MLS): a mean profile characterizing the summer season of mid-latitudes regions falling between  $22^\circ$  and  $45^\circ$ .
- Profile « Mid Latitude Winter » (MLW): a mean profile characterizing the winter season of mid-latitudes regions falling between  $22^\circ$  and  $45^\circ$ .
- Profile « High Latitude Summer » (HLS): a mean profile characterizing the summer season of high-latitudes regions situated above  $45^\circ$ .
- Profile « High Latitude Winter » (HLW): a mean profile characterizing the winter season of high-latitudes regions situated above  $45^\circ$ .

The vertical profiles of pressure and temperature of these reference atmospheres are depicted in Figure 5.

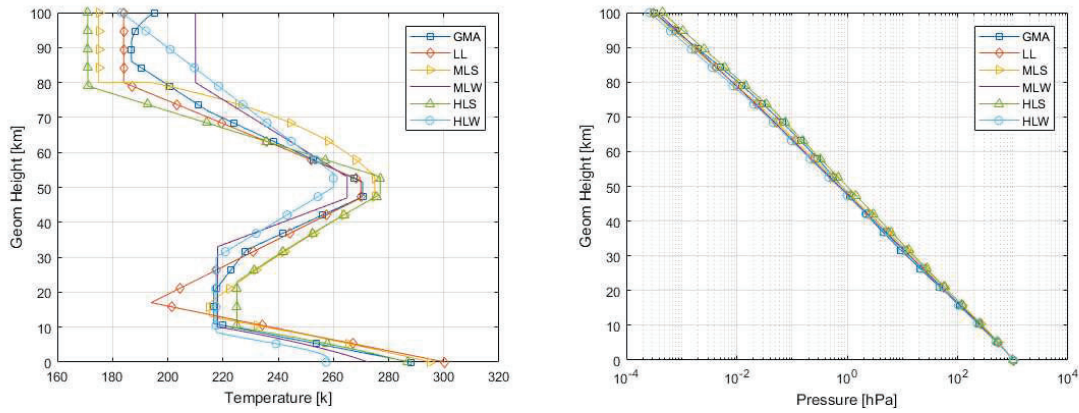


Figure 5 : Reference atmospheres: temperature profiles (left), pressure profiles (right)

Using the definition of refractive index in (20), we derive the corresponding vertical profiles of refractive index as depicted in Figure 6 for a wavelength  $\lambda = 1.55\mu m$ .

The refractive index is significantly different for the first kilometer between the reference atmospheres but at higher altitudes, the refractive indexes tend to be similar.

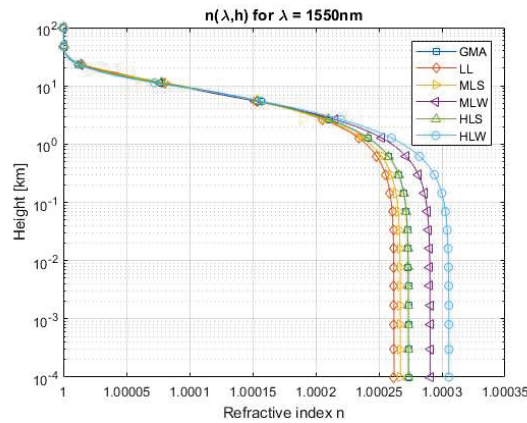


Figure 6 : Reference refraction profiles for  $\lambda = 1.55\mu m$

#### 4. RESULTS AND DISCUSSIONS

For illustration purposes, we consider the practical case of a LEO satellite at  $H_{SAT} = 600 km$ . The DTE LEO wavelength configuration is as follows:

- Two possible beacon (pointing) wavelengths : in the visible range  $\lambda_p = 500 nm$  and in the IR  $\lambda_p = 808 nm$
- A downlink transmission wavelength  $\lambda_t = 1550 nm$

The geometric elevation angle  $\theta_{geo}$  ranges between  $5^\circ$  and  $90^\circ$ .

For each geometric elevation angle, and for each reference atmosphere, we compute the observed elevation and nadir angles by successive launching of rays using dichotomy and numerically solving the integrals in (16) and (20). The dichotomy stops when the criteria of equations (14) and (17) is reached, which numerically writes as:

$$|\phi_{obs}(\theta_{obs} \text{ or } \psi_{obs}) - \phi_{geo}|^2 < 10^{-16} [^\circ]^2 \quad (21)$$

In a first part of the analysis, we compared the observed elevation and nadir angles with their geometrical values in order to assess the impact of atmospheric refraction on the transmission wavelength as depicted in Figure 7 and Figure 8.

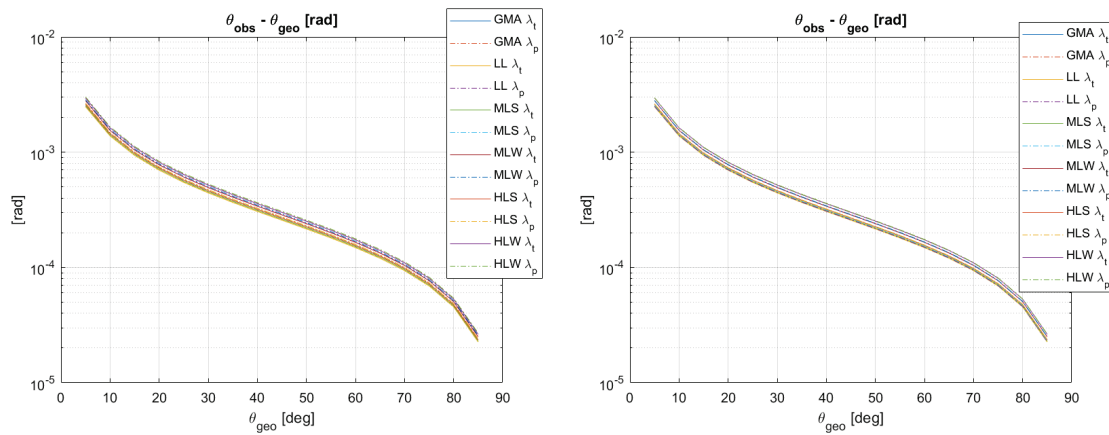


**Figure 7 : Difference between elevation angles with and without refraction for:  $\lambda_t = 1550nm$  and  $\lambda_p = 500nm$  (left),  $\lambda_p = 808nm$  (right)**

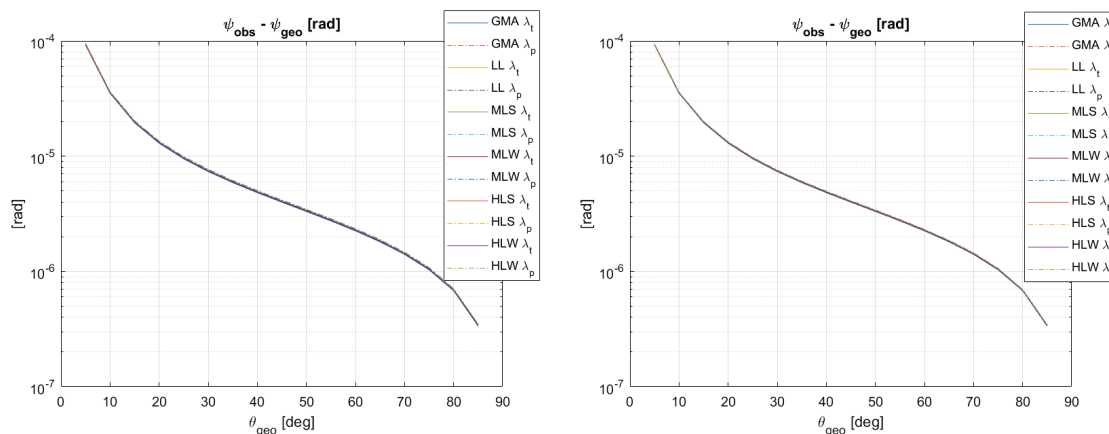


**Figure 8 : Difference between nadir angles with and without refraction for:  $\lambda_t = 1550nm$  and  $\lambda_p = 500nm$  (left),  $\lambda_p = 808nm$  (right)**

It can be noticed that, for both elevation and nadir angles, the difference with geometrical angles is almost agnostic of the nature of the refraction profile. Moreover, as expected, the observed elevation and nadir angles are higher than their geometrical counterparts, which is due to the decreasing refractive index profiles.

As far as the elevation angle is considered, the difference between geometrical and observed values can reach few *mrad* for low geometrical elevations. This difference reduces with increasing elevation and reaches few tens of  $\mu rad$  near zenith.

Regarding the observed nadir angle, the difference between geometrical and observed values is lower by a decade compared to the variations of elevation angles. This is due to the geometry of the link, where the atmospheric refraction takes place mostly near the ground (few tens of kilometers), making the link more sensitive to refraction from the OGS point of view (elevation angle) than from the satellite point of view (nadir angle). The difference in nadir angles can vary between hundreds of  $\mu rad$  for low elevation angle to sub- $\mu rad$  difference near zenith.

In terms of wavelength dependence, although Figure 7 and Figure 8 may macroscopically show no dependence on the wavelength, the difference between angles for the considered wavelengths can be quite significant as shown in Figure 9 and Figure 10.

As expected, the negative sign of the difference between angles at  $\lambda_t = 1550 \text{ nm}$  compared to both  $\lambda_p = 500 \text{ nm}$  and  $\lambda_p = 808 \text{ nm}$  reflects the decreasing monotony of equation (20), where  $\theta_{obs}(\lambda_t = 1550 \text{ nm}) < \theta_{obs}(\lambda_p = 808 \text{ nm}) < \theta_{obs}(\lambda_p = 500 \text{ nm})$ .

Moreover, the absolute value of these differences tends to decrease with increasing geometrical angle since the impact of refraction decreases with higher elevation. What is more important is that the difference between observed elevation angles at different wavelengths can reach values from ten to several tens of  $\mu\text{rad}$  at low elevation angle. This implies that the pointing of the OGS towards the satellite may be different by few tens of microns w.r.t to the observed angle when the signal is transmitted at wavelength  $\lambda_t = 1550 \text{ nm}$ .

The differences between elevation angles at the transmission wavelength and the pointing wavelength can reach up to 60  $\mu\text{rad}$  for ( $\lambda_p = 500\text{nm}$ ) and 20  $\mu\text{rad}$  for  $\lambda_p = 808 \text{ nm}$ .

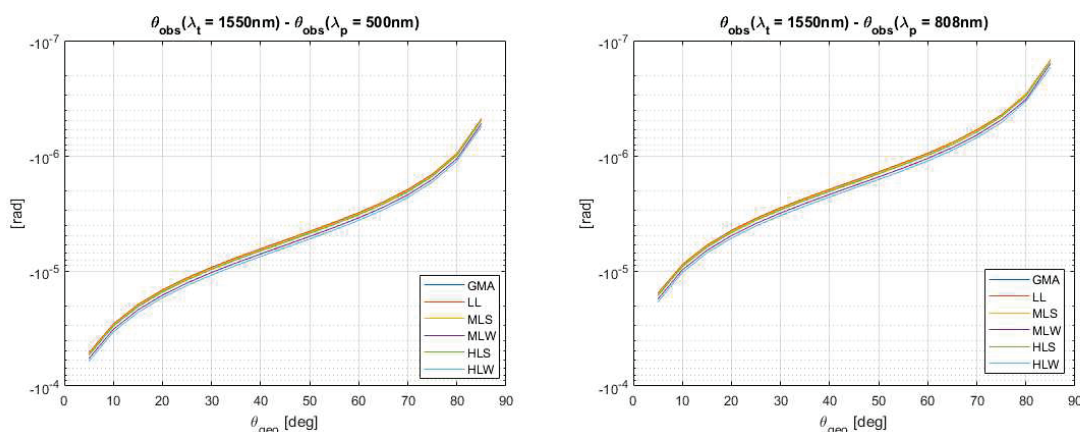


**Figure 9: Difference between observed elevation angles for:  $\lambda_t = 1550 \text{ nm}$  and  $\lambda_p = 500 \text{ nm}$  (left),  $\lambda_p = 808 \text{ nm}$  (right)**

Figure 10 presents the difference between the nadir angles for  $\lambda_t = 1550 \text{ nm}$  compared to both  $\lambda_p = 500 \text{ nm}$  and  $\lambda_p = 808 \text{ nm}$ . The difference between observed nadir angles at transmission and pointing wavelengths is lower than the difference of observed elevation angles. Besides, the difference of nadir angles can reach 2  $\mu\text{rad}$  at geometrical elevation  $5^\circ$ .

## 5. CONCLUSIONS

This paper has presented a theoretical framework for the computation of both elevation and nadir angles taking into account atmospheric refractivity. Different index of refraction profiles have been defined building on the ITU reference atmospheric profiles as well as a state of the art optical refraction index model. The computed refracted elevation and nadir angles have been compared for different pointing wavelengths  $\lambda_p = 500 \text{ nm}$  and  $\lambda_p = 808 \text{ nm}$  with regard to the equivalent angles at a transmission wavelength  $\lambda_t = 1550\text{nm}$ . Results show negligible dependence on the climate type but substantial difference between the communication link and the pointing beacon as summarized in the following table for a  $5^\circ$  geometric elevation angle. These differences can have implications depending on the pointing strategies as well as the field of view of both OGS and satellite detectors.

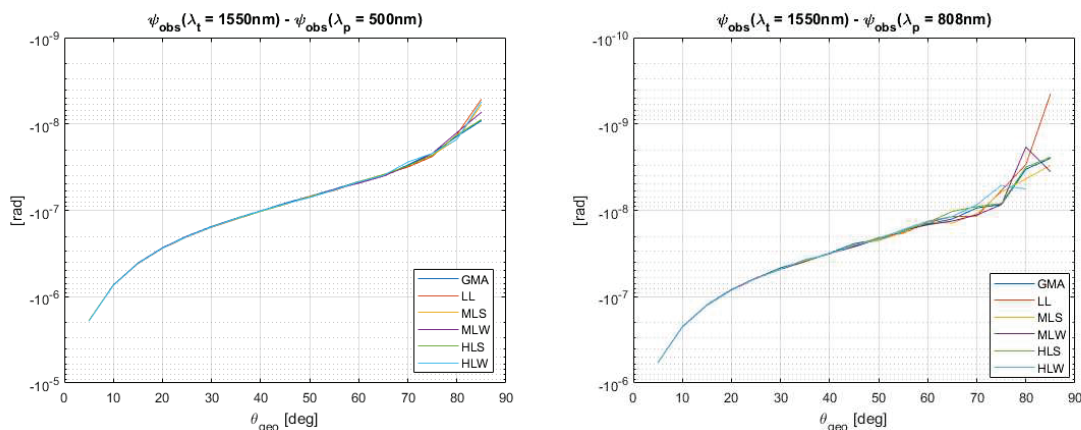


Figure 10: Difference between observed nadir angles for:  $\lambda_t = 1550 \text{ nm}$  and  $\lambda_p = 500 \text{ nm}$  (left),  $\lambda_p = 808 \text{ nm}$  (right)

Table 1: Difference in observed elevation and nadir angles for  $\lambda_t = 1.55 \mu\text{m}$  and geometrical link elevation  $\theta_{geo} = 5^\circ$

Pointing wavelength	Elevation : $\theta_{obs}(\lambda_t) - \theta_{obs}(\lambda_p)$	Nadir : $\Psi_{obs}(\lambda_t) - \Psi_{obs}(\lambda_p)$
$\lambda_p = 500 \text{ nm}$	$60 \mu\text{rad}$	$2 \mu\text{rad}$
$\lambda_p = 808 \text{ nm}$	$20 \mu\text{rad}$	$0.6 \mu\text{rad}$

## 6. REFERENCES

- [1] Recommendation ITU-R P.1621-2 “Propagation data required for the design of Earth-space systems operating between 20 THz and 375 THz”. *International Telecommunication Union, radiocommunication sector.*
- [2] Recommendation ITU-R P.676-12 “Attenuation by atmospheric gases and related effects”. *International Telecommunication Union, radiocommunication sector.*
- [3] Lin, L., Chen, X., Hu, R., & Zhao, Z. (2020). The refraction correction of elevation angle for the mean annual global reference atmosphere. *International Journal of Antennas and Propagation, 2020.*
- [4] Purvinskis, R., Giggenbach, D., Henniger, H., Perlot, N., & David, F. (2003, July). Multiple-wavelength free-space laser communications. In *Free-Space Laser Communication Technologies XV* (Vol. 4975, pp. 12-19). SPIE.
- [5] Allen, C. W. (1973). *Astrophysical quantities.* United Kingdom.
- [6] Recommendation ITU-R P.453-14 “The radio refractive index: its formula and refractivity data”. *International Telecommunication Union, radiocommunication sector.*
- [7] Recommendation ITU-R P.835-6 “Reference standard atmospheres”. *International Telecommunication Union, radiocommunication sector.*